View metadata, citation and similar papers at core.ac.uk

brought to you by CORE

provided by Digital.CSIC

Attostreaking with metallic nano-objects

This article has been downloaded from IOPscience. Please scroll down to see the full text article.

2012 New J. Phys. 14 023036

(http://iopscience.iop.org/1367-2630/14/2/023036)

View the table of contents for this issue, or go to the journal homepage for more

Download details:
IP Address: 158.227.173.8
The article was downloaded on 16/02/2012 at 11:39

Please note that terms and conditions apply.

New Journal of Physics
The open-access journal for physics

Attostreaking with metallic nano-objects

A G Borisov[1,6], **P M Echenique**[2,3,4] **and A K Kazansky**[2,4,5]

[1] Institut des Sciences Moléculaires d'Orsay (ISMO), UMR 8214, CNRS-Université Paris-Sud, Bât. 351, Université Paris-Sud, 91405 Orsay Cedex, France
[2] Depto de Física de Materiales, Facultad de Ciencias Químicas, UPV/EHU, 20018 San Sebastián/Donostia, Spain
[3] Centro de Física de Materiales (CFM), UPV/EHU, 20018 San Sebastián/Donostia, Spain
[4] Donostia International Physics Center (DIPC), Paseo Manuel de Lardizabal 4, 20018 San Sebastián/Donostia, Spain
[5] IKERBASQUE, Basque Foundation for Science, 48011 Bilbao, Spain
E-mail: andrei.borisov@u-psud.fr

New Journal of Physics **14** (2012) 023036 (16pp)
Received 20 July 2011
Published 15 February 2012
Online at http://www.njp.org/
doi:10.1088/1367-2630/14/2/023036

Abstract. The application of atto-second streaking spectroscopy (ASS) to direct time-domain studies of the plasmonic excitations in metallic nano-objects is addressed theoretically. The streaking spectrograms for a rectangular gold nano-antenna and spherical gold clusters are obtained within strong field approximation using classical electron trajectory calculations. The results reported here for spherical clusters are also representative of spherical nano-shells. This study demonstrates that ASS allows for detailed characterization of plasmonic modes, including near-field enhancement, frequency and decay rate. The role of the inhomogeneity of the induced electric fields is also demonstrated.

[6] Author to whom any correspondence should be addressed.

© IOP Publishing Ltd and Deutsche Physikalische Gesellschaft

Contents

1. Introduction

For metallic nano-objects, the collective plasmonic response of the conduction band electrons to external electromagnetic radiation leads to a large near-field enhancement [1, 2]. Because of its practical and fundamental interest, this phenomenon has been the focus of thorough research as evidenced by a number of recent reviews [3–7]. Information technology [8, 9], optical nano-antennas [10, 11] allowing, in particular, single-molecule detection [12–14], energy transfer with nano-particle arrays [15–17], and coherent control of the field enhancement within a spot much smaller than the radiation wavelength [18–20] are some examples of the subjects covered by the fast growing field of nano-plasmonics. A comprehensive understanding of the dynamics of electrons in nano-systems would help not only in the characterization of existing devices, but also in the search for future ones. Most of the available experimental probes provide detailed information on the optical near-field in metallic nano-objects in the stationary regime, i.e. on long time scales as compared to the plasmon period [21–25]. The pump–probe techniques with femtosecond (fs) laser pulses allow one to address issues such as plasmon propagation or relaxation and dephasing [26–31], but still do not have sufficient resolution to observe directly the plasmonic fields in the time domain.

In this context, the development of the sub-femtosecond experimental technique [32] initiated in 2001 provides a prospective tool for monitoring electron dynamics in nano-systems. By keeping track of the temporal evolution of outgoing electron wave packets, this technique has been shown to give direct time-domain insight into various aspects of the interaction of an electron with non-stationary many-electron systems. First, atto-second streaking spectroscopy (ASS) enabled the observation of the decay of an inner-shell vacancy through Auger relaxation in isolated atoms in the gas phase [33]. In this as well as in most other experiments with atto-second pulses, the time dynamics was observed with an ingenious 'streaking camera' [34–40]. The infrared (IR) pulse, which produces the atto-second pulse by high-harmonics generation, is simultaneously used to transpose the electron ejection time into the electron energy spectrum (for details, see below). Another type of studies with atto-pulses, the so-called 'atto-chronoscopy' [41–43] that does not use the streaking idea, deserves to be mentioned. Until now, experiments have been performed mostly on free atoms in the gas phase (for a review, see [40]). The first experimental extension of the atto-second streaking technique to processes with solid surfaces was done only recently [44]. This important experiment has shown that it is possible to obtain direct time-domain access to charge dynamics at the near-surface region of metals by probing photoelectron emission from a single crystal. Regarding

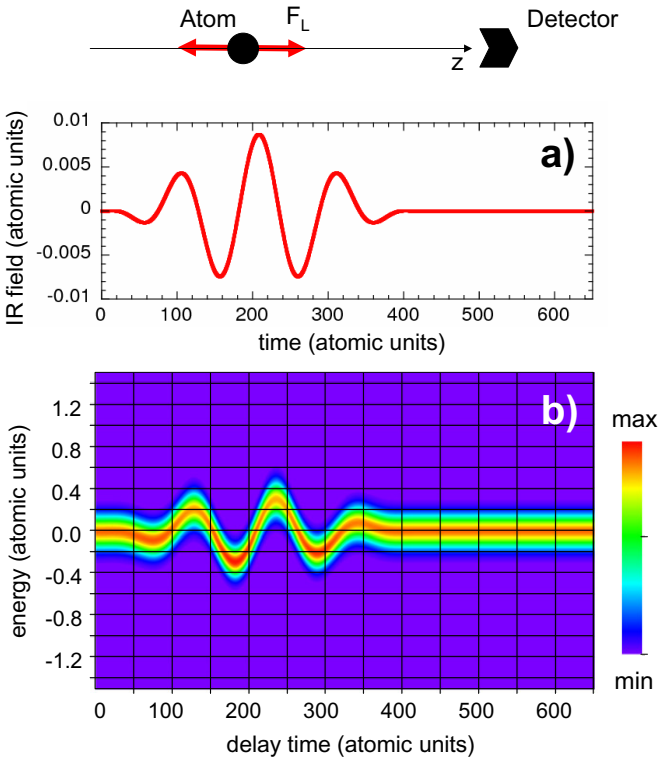

Figure 1. Atto-second streaking spectrogram for the free atom. Upper panel sketches the scheme of the experiment. (a) The time evolution of the electric field of the IR laser pulse. (b) Final streaking spectrogram. The energy spectrum of ejected electrons is shown as function of the delay time t_d. The color code defines the intensity of the signal as shown in the insert. The energies are given with respect to the central line $E_f = 2$ au.

the nano-objects, to the best of our knowledge, no experiments with atto-pulses have been performed so far.

In this paper, we theoretically study the application of the streaking technique for the characterization of plasmonic near-fields of metallic nano-objects such as optical nano-antenna and spherical nano-clusters of different sizes. We show that the external IR field enhancement near the nano-object reveals itself in a large amplitude of the streaking oscillations. Moreover, our results demonstrate that ASS allows detailed characterization of the plasmonic mode excited by the external IR field. The frequency, decay rate and phase of the plasmon oscillation can be directly measured in the time domain. Thus, ASS can become a very important tool for investigating the plasmonic dynamics of nano-objects.

2. Basic equations and approximations

The 'streaking camera' scheme was invented for the investigation of the reaction of atoms on the atto-second pulse and for the control of the characteristics of this pulse [40]. We first consider the typical implementation of the method for the free-atom case (figure 1). The corresponding streaking spectra will be used as the reference to unravel the role of plasmonic excitations in

nano-objects. The uniform IR laser pulse is incident at the atom. The electric field of the pulse is polarized along the z-axis, and it is given by (atomic units are used everywhere unless otherwise stated) [45]

$$\mathbf{F}_{\mathrm{L}}(t) = \hat{\mathbf{e}}_z \frac{F_0}{2} \left\{ \cos\left[\frac{2\pi t}{\tau_{\mathrm{L}}} - \pi \right] + 1 \right\} \cos\left[\omega_{\mathrm{L}} \left(t - \frac{\tau_{\mathrm{L}}}{2} \right) \right]. \tag{1}$$

In equation (1), $\hat{\mathbf{e}}_z$ is the unit length vector along the z-axis. $\omega_{\mathrm{L}} = 1.6\,\mathrm{eV}$ is the frequency of the pulse, $\tau_{\mathrm{L}} = 10\,\mathrm{fs}$ (420 au) is the pulse duration, and the pulse intensity is $10^{12}\,\mathrm{W\,cm^{-2}}$ (the corresponding amplitude of the electric field: $F_0 = 8.717 \times 10^{-3}$ au). The z-polarized atto-second pulse,

$$\mathbf{F}_{\mathrm{as}}(t) = \hat{\mathbf{e}}_z F_{\mathrm{as}}\, \mathrm{e}^{-(t-t_{\mathrm{d}})^2/\Delta^2} \cos[\omega_{\mathrm{as}}(t - t_{\mathrm{d}})]\,, \tag{2}$$

comes with some time delay t_{d} with respect to the onset of the IR pulse. $\Delta = 0.4\,\mathrm{fs}$ (16.8 au) is the duration, and F_{as} is the (small) amplitude of the atto-second pulse, $\omega_{\mathrm{as}} = 100\,\mathrm{eV}$. The atto-second pulse ejects an electron from the atom. After the electron ejection, the IR field acts on the outgoing electron and changes its energy. The observed final energy spectrum of the emitted electrons depends on the delay time t_{d} and this dependence allows one to probe the result of the atto-second ionization in the time domain.

For simplicity, we consider the ionization of a deep atomic s-shell with an energy E_{s} such that in the absence of the IR field, the final energy of the photo-emitted electron is $E_{\mathrm{f}} = E_{\mathrm{s}} + \omega_{\mathrm{as}} = 2\,\mathrm{au}$. The direction of the electron ejection is determined by the conventional rules of one-photon absorption in a free atom, which leads to a certain angular distribution of the ejected electrons. Experimentally, the electrons ejected in a small cone about the direction of polarization of the incident atto-second pulse are usually the object of measurement. Thus we restrict ourselves to the observation of electrons ejected along the z-axis so that the simplified treatment can be used.

A key idea of the streaking effect is that the electron ejected from an atom by the atto-pulse acquires additional velocity from the strong IR field. Within the strong-field approximation, the final velocity of the electron photo-emitted at the instant of time t_{d} along the z-axis is given by

$$v_z(t_{\mathrm{d}}) = u - \int_{t_{\mathrm{d}}}^{\infty} F_{\mathrm{L}}(t)\,\mathrm{d}t, \tag{3}$$

where $u = \sqrt{2E_{\mathrm{f}}}$ is the initial velocity of the emitted electron. Introducing the vector potential of the IR laser field A_{L}:

$$A_{\mathrm{L}}(t) = \int_{t}^{\infty} F_{\mathrm{L}}(t')\,\mathrm{d}t', \tag{4}$$

equation (3) can be expressed as

$$v_z(t_{\mathrm{d}}) = u - A_{\mathrm{L}}(t_{\mathrm{d}}). \tag{5}$$

The corresponding final kinetic energy of the ejected electron reads

$$E(t_{\mathrm{d}}) = E_{\mathrm{f}} - u A_{\mathrm{L}}(t_{\mathrm{d}}) + \frac{1}{2}\left[A_{\mathrm{L}}(t_{\mathrm{d}})\right]^2. \tag{6}$$

Equation (6) is widely used to discuss streaking experiments with atoms in the gas phase.

Thus, the final electron energy distribution reveals dependence of the process on the time of electron ejection t_{d}. Basically, it reflects the time evolution of $A_{\mathrm{L}}(t_{\mathrm{d}})$, the last term in equation (6)

being conventionally rather small. This simple streaking curve has to be averaged over the possible initial conditions $u = \sqrt{2(E_s + \omega)}$ produced by the ω-spectrum of the atto-pulse. For this averaging we use the Gaussian distribution:

$$G = \exp(-(u^2/2 - E_f)^2/\delta^2), \qquad \delta = \sqrt{(2/\Delta)^2 + 2E_f F_L^2(t_d)}, \tag{7}$$

centered at E_f with the effective spectral width δ. The term $2/\Delta$ ($\approx$3.2) eV in equation (7) is the spectral width of the atto-second pulse. It is worth noting that the quantities E_s and ω_{as} do not enter our study explicitly; instead we use the central value of the ejected electron energy $E_f = 2$ au. The representation of the effective width in the emitted electron energy distribution was obtained in [34] by the analysis of the semiclassical approximation for the strong-field approximation and confirmed in [46] with fully quantum computations. Averaging the result of computations with equation (6) over the energy distribution of the emitted electrons, one obtains the streaking spectrogram for the free-atom case shown in figure 1.

In the case of a metal nano-particle, the total IR field acting on the emitted electron is a sum of the incident and the induced fields:

$$\mathbf{F}_{IR}(\mathbf{r}, t) = \hat{\mathbf{e}}_z F_L(t) + \mathbf{F}_{ind}(\mathbf{r}, t). \tag{8}$$

Here, $\mathbf{F}_{ind}(\mathbf{r}, t)$ is the field created by the nano-particle in response to the incident IR pulse. In contrast to F_L, the induced field $\mathbf{F}_{ind}$ is spatially non-homogeneous and depends explicitly on the coordinates $\mathbf{r}$. Thus, equations (2)–(5) describing the streaking effect for the free-atom case have to be generalized as follows:

$$\begin{aligned} &\frac{d\mathbf{v}(\mathbf{r}_0, t)}{dt} = -\mathbf{F}_{IR}(\mathbf{r}(t), t), \qquad \mathbf{v}(\mathbf{r}_0, t_d) = \hat{\mathbf{e}}_u u, \\ &\frac{d\mathbf{r}(t)}{dt} = \mathbf{v}(\mathbf{r}_0, t), \qquad \mathbf{r}(t_d) = \mathbf{r}_0, \\ &E(t_d) = |\mathbf{v}(\mathbf{r}_0, t = \infty)|^2/2. \end{aligned} \tag{9}$$

In equation (9), $\hat{\mathbf{e}}_u$ is the unit length vector defining the initial direction of motion for the ejected electron. The probability distribution of the initial ejection angles is given by the corresponding dipolar matrix elements. In the case of a dense matter, the atto-second XUV pulse penetrates the object and can eject electrons from any atom located at position $\mathbf{r}_0$ within the object. However, the inelastic mean free path of 50 eV electrons in a metal is, as a rule, rather short, being in the 5 Å range [47]. Then, only the electrons ejected from surface adatoms or atoms in the surface layer of the nano-particle can reach the detector carrying non-distorted information on the ejection process. A similar situation has been discussed previously in relation to the experimental study of the interaction of atto-second pulses with electrons in metals [48].

In order to calculate the streaking spectrogram, a large number of electron trajectories have to be used with initial conditions that sample different launch positions at the surface of the nano-particle $\mathbf{r}_0$, different initial ejection angles $\hat{\mathbf{e}}_u$, as well as possible energies of the emitted electron. The energy sampling is performed with the distribution function given by equation (7), where the effective spectral width δ is computed not with the field of the incident IR pulse $F_L(t_d)$, but with the total electric field $F_{IR}(\mathbf{r}_0, t_d)$ at the point and the moment of the electron emission. Since we are interested in the gross features of the effect of the plasmonic fields on the streaking

spectra, the simplified treatment is used in our computations. Indeed, for the registration of the electrons emitted along the z-axis the final velocity should satisfy

$$\mathbf{v}(\mathbf{r}_0, t = \infty) = \hat{\mathbf{e}}_z |\mathbf{v}(\mathbf{r}_0, t = \infty)|. \tag{10}$$

Taking into account the large initial velocity $u = 2$ au, only electrons ejected close to the z-axis will be detected. We thus consider only the z-component of the total IR field $\mathbf{F}_{\rm IR} \to \hat{\mathbf{e}}_z(\hat{\mathbf{e}}_z \cdot \mathbf{F}_{\rm IR})$ in equation (9), and assume that the electron is initially ejected along the z-axis $\hat{\mathbf{e}}_u = \hat{\mathbf{e}}_z$. The x- and y-component of $\mathbf{F}_{\rm IR}$ lead only to a slight deflection of a trajectory, which has to be compensated for by a very small variation of the initial ejection angle $\hat{\mathbf{e}}_u$ so that equation (10) is fulfilled.

When the spectrum of the incident IR pulse overlaps the nano-particle plasmon, the latter can be efficiently excited, leading to a strong near-field enhancement. In this case, $\mathbf{F}_{\rm IR}(\mathbf{r}, t)$ is dominated by the induced plasmonic field which reveals itself in the streaking spectrograms. With examples discussed below, our study shows that ASS offers a time-domain insight into plasmonic dynamics.

3. Streaking with metallic nano-objects

In what follows we present a proof-of-principle study of the streaking effect with an atom placed on the surface of a nano-object. The goal of this work is to demonstrate the streaking effect in the plasmonic field of the nano-object. The initial state of the electron in the atom is assumed to be spherically symmetric. We take the XUV photon energy to be large enough so that the final energy of the electron after absorption of this photon is centered at 2 au. This allows us, in the first approximation, to neglect the polarization of the final electron state by the cluster potential. In our computations, we consider the electron emission only from the atoms at the surface of the nano-particle since the inelastic mean free path in the considered energy interval is of the order of inter-atom distance.

3.1. Rectangular gold nano-antenna

We first consider the gold nano-antenna with rectangular $40 \times 40 \times 180$ nm geometry, sketched in figure 2. The z-axis is directed along the longest side of the antenna. The total IR field has been computed with a rigorous time-domain pseudo-spectral solver of the Maxwell equations [49]. The dielectric function of gold within the frequency range of interest can be well described within the Drude model $\varepsilon_{\rm Au}(\omega) = 1 - \omega_{\rm p}^2/[\omega(\omega + {\rm i}\eta)]$ with the plasma frequency $\omega_{\rm p} = 7.9$ eV and attenuation $\eta = 0.09$ eV [50]. The calculated nano-antenna response is characterized by the dipolar plasmon resonance at $\Omega = 1.48$ eV close to the frequency of the incident IR pulse. The calculated width of the resonance is $\Gamma = 0.2$ eV, i.e. the corresponding induced dipole decays in time as $\exp[-\Gamma t/2]$ with $\Gamma/2 = 0.1$ eV.

Figure 2 shows snapshots of the z- and y-components of the field induced in response to the incident IR pulse. The excitation of the dipolar plasmon mode oriented along the z-axis clearly follows from the structure of the induced fields shown in the figure. The z-component of the IR field is strongly enhanced in the vicinity of the nano-antenna with the enhancement factor close to 6. (This factor is a ratio between the z-component of the total IR field and that of the incident IR field.) Outside the z-extremities of the antenna, the F_z component of the field relevant for our study shows a z-dependence with a characteristic scale in the 10 nm range. An electron ejected

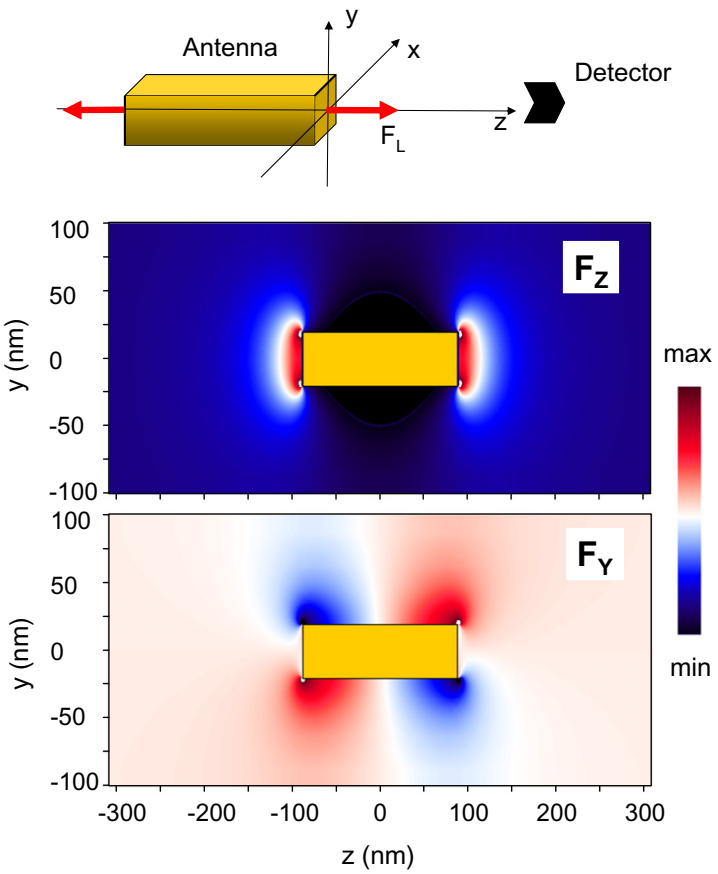

Figure 2. Rectangular gold nano-antenna. The upper panel sketches the scheme of the atto-second streaking experiment and the geometry of the system. Middle panel: the component of the induced IR field along the z-axis. Calculated results are shown in the $(x = 0, y, z)$-plane as a function of the y- and z-coordinates. The color code is given in the inset. Lower panel: the same as the middle panel, but for the y-component of the induced IR field.

from the surface atom with initial velocity 2 au needs $\mathbb{T} = 100$ au (2.4 fs) to 'explore' the spatial variation of the induced field created by the nano-object. We recall that the period of the IR field with the frequency $\omega_L = 1.6$ eV is $T_L = 107$ au (2.5 fs). The two characteristic time scales being comparable, both spatial and temporal variations of the fields contribute to the final streaking spectra, as calculated with equation (9). In this respect, the present situation is quite different from the instantaneous emission regime $\mathbb{T} \ll T_L$ considered in the proposal for an atto-second nano-plasmonic-field microscope in [51, 52]. The latter requires either extremely well-localized plasmonic near-fields or a much higher energy of the emitted electron.

In figure 3, we show the atto-streaking spectrogram for the rectangular gold nano-antenna. The results presented in this figure include the emission energy statistics determined by the frequency spectrum of the XUV atto-second pulse. Calculations are performed under the assumption that, because of the inelastic electron–electron scattering effects, only the electrons emitted from the face of the nano-antenna located in front of the detector contribute to the final result. The streaking effect is clearly seen in the figure. Analysis of the delay-time characteristics

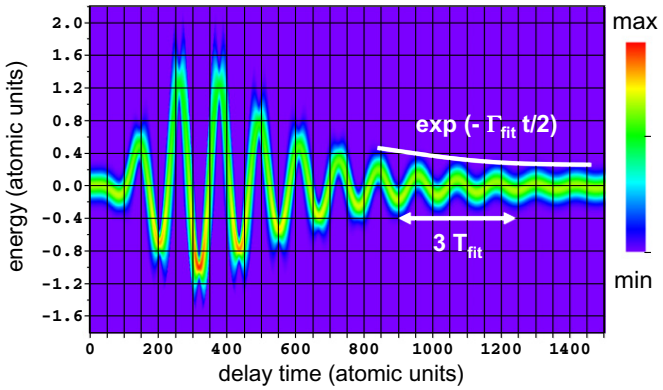

Figure 3. Calculated streaking spectrogram for the rectangular gold nano-antenna. The energy spectrum of ejected electrons is shown as a function of the delay time t_d. The color code defines the intensity of the signal as shown in the inset. The energies are given with respect to the central line $E_f = 2$ au. At large delay times, the period and decay rate of the dipolar plasmonic mode of the nano-antenna can be extracted from the streaking spectrogram as shown in the figure.

of the streaking spectrogram and its comparison with the free-atom case (see figure 1) allows one to access the characteristics of the plasmonic fields.

1. The amplitude of the energy oscillations for the rectangular nano-antenna is approximately three times larger than for the free-atom case, which reflects a near-field enhancement. The enhancement factor of 3 deduced from the streaking spectra is lower than the enhancement factor of 6 obtained directly from the calculated electromagnetic field in the vicinity of the nano-antenna face. It is the finite spatial extension of the near field probed by the outgoing electron (see discussion above) that reduces the 'apparent' field enhancement.
2. Close inspection of the free-atom and nano-antenna streaking spectrograms reveals that the oscillating structure of the latter is delayed by $\pi/2$ with respect to the former. Indeed, because of the field enhancement, the streaking spectrum of the nano-antenna is determined primarily not by the incident pulse, but by the resonantly excited plasmonic field of the nano-antenna. In the conditions of the near-resonant excitation the induced IR field is delayed by $\pi/2$ with respect to the driving incident IR pulse.
3. At large delay times t_d the streaking signal shows an exponentially damped oscillating structure, which lasts much longer than the duration of the initial IR pulse (i.e. 420 au). Indeed, at large t_d the IR field acting on the ejected electron is fully determined by the dynamics of the excited antenna resonance. Analyzing the streaking signal after the termination of the incident IR pulse (see the sketch in figure 3), one can extract the characteristics of the time evolution of the plasmonic field. Thus, the extracted resonance period $T_{fit} = 115$ au corresponds to the resonance frequency $\Omega_{fit} = 1.49$ eV. The agreement with $\Omega = 1.48$ eV obtained by the direct calculation of the electromagnetic fields is excellent. Similarly, the rate of the exponential decay $\Gamma_{fit}/2 = 0.12$ eV extracted from the streaking spectra agrees well with the exact 0.1 eV value.

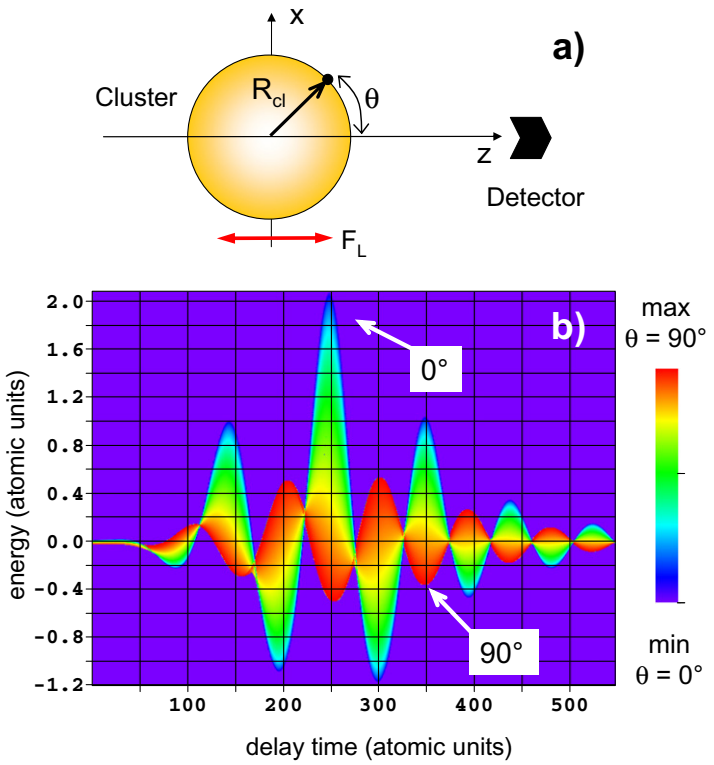

Figure 4. Atto-second streaking for spherical gold cluster, $R_{\mathrm{cl}} = 50\,\mathrm{nm}$. (a) Sketch of the scheme of the experiment and the geometry of the system. Angle θ defines the electron emission point at the surface of the cluster. (b) Ensemble of streaking curves obtained for electrons ejected from different portions of the cluster surface defined by the angle θ. The initial velocity of the ejected electron is $u = 2\,\mathrm{au}$ along the z-axis. Results are shown as function of the energy and delay time t_{d}. The energies are given with respect to the central line $E_{\mathrm{f}} = 2\,\mathrm{au}$. The color code is defined at the insert of the figure. It is given by the weighting factor $\sin(\theta)$ and reflects the number of equivalent emitters at the surface of the cluster contributing to the given streaking curve. The streaking curves for $\theta = 0$ and $\theta = \pi/2$ delimiting the spectra are explicitly labeled.

3.2. Spherical gold clusters

In the case of the rectangular nano-antenna, the electrons emitted from the face of the nano-antenna and reaching the detector all move in nearly the same induced electromagnetic field, which explains the well-resolved streaking spectra. However, for nano-objects of general geometry, due to the spatial inhomogeneity of the induced field, the emitted electrons will experience different streaking in dependence on the launch position at the surface of the nano-object. This is the case for the streaking spectrometry performed on spherical metallic nano-clusters as sketched in figure 4. The IR and atto-second pulse, both polarized along the z-axis, are incident on a gold nano-sphere of radius R_{cl}. The electrons are ejected from the atoms (or adatoms) located at the surface of the nano-sphere facing the detector. The electron ejection point is thus defined by the azimuth angle φ $(0 \leqslant \varphi \leqslant 2\pi)$ and polar angle θ $(0 \leqslant \theta \leqslant \pi/2)$

in spherical coordinates with the z-axis as indicated in figure 4(a) and coordinate origin at the middle of the cluster. Since we observe the ejected electrons only along the z-axis, we restrict calculations to only this initial direction of the electron velocity. For a given emission point, the final kinetic energy of the ejected electron is obtained from equations (9). The IR field induced by the spherical cluster is calculated within the non-retarded approximation, which is well justified for the purpose of the present proof-of-principle study and for the characteristic distance scales and nano-sphere sizes studied here.

We considered gold clusters with $R_{\rm cl} = 50\,$nm and $R_{\rm cl} = 20\,$nm, i.e. much smaller than the characteristic wavelength of the IR pulse. Experimentally measured [53] and calculated [54] optical responses of these size particles are dominated by the well-defined dipolar plasmon resonance. The spectrum of the induced dipole along the z-axis $\tilde{P}(\omega)$ can then be described as [1, 54]

$$\tilde{P}(\omega) = -R_{\rm cl}^3 \frac{\Omega^2}{\omega^2 + {\rm i}\omega\Gamma - \Omega^2} \tilde{F}_{\rm L}(\omega), \tag{11}$$

where $\tilde{F}_{\rm L}(\omega)$ is the spectrum of the external laser field, Ω is the dipolar plasmon resonance frequency and Γ is the width of the resonance. For larger size clusters the higher-order multipolar modes become increasingly important because of the retardation effects [54]. This can be accounted for within Mie theory [55]. We emphasize, however, that this paper focuses on the gross effects of plasmonic excitations, as can be observed with atto-second streaking experiments. Thus, we leave the fine effects due to multipolar terms for a future study.

In order to model the realistic cluster response, including radiation losses and many-body damping [56], we used empirical data for the frequency Ω and width Γ of the dipolar plasmon resonance. From the measured optical properties of spherical gold clusters with diameters of 20 nm and larger [53], one obtains: $\Omega = 2.0\,$eV and $\Gamma = 0.5\,$eV for $R_{\rm cl} = 50\,$nm; and $\Omega = 2.2\,$eV and $\Gamma = 0.3\,$eV for $R_{\rm cl} = 20\,$nm. Replacing in equation (11) ω by ${\rm i}\partial/\partial t$, the time evolution of the induced dipole can be obtained by solving the differential equation

$$\frac{\partial^2 P(t)}{\partial t^2} + \Gamma \frac{\partial P(t)}{\partial t} + \Omega^2 P(t) = R_{\rm cl}^3 \Omega^2 F_{\rm L}(t). \tag{12}$$

The z-component of the induced IR field relevant for our study $\hat{\mathbf{e}}_z \cdot \mathbf{F}_{\rm ind}(\mathbf{r}, t)$ is then given by

$$\hat{\mathbf{e}}_z \cdot \mathbf{F}_{\rm ind}(x, y, z, t) = \frac{2z^2 - (x^2 + y^2)}{r^5} P(t). \tag{13}$$

It is worth noting that as in the metal nano-antenna case, only the electrons emitted from the surface of the cluster facing the detector are recorded. This is because of the inelastic effects leading to the short mean free path of electrons inside the metal. As a direct consequence, the results obtained here for small spherical clusters (see below) are representative also of small spherical metallic nano-shells under the excitation of both bonding and anti-bonding plasmon modes of dipolar character [57, 58]. Indeed, while the absolute values of the fields at resonance differ, the induced field structure above the surface is given by equation (13), i.e. it is the same for the nano-shell and the nano-cluster. The nano-shells attract much interest because of the tunability of the plasmonic resonance over a wide range of frequencies [7, 57–61].

The dependence of the streaking effect on the electron ejection point, i.e. on the position of the photo-ionized atom at the surface of the cluster, is shown in figure 4(b) for $R_{\rm cl} = 50\,$nm. To show the effect of the inhomogeneity of the IR field, we assume homogeneous distribution of the intensity of the atto-second XUV pulse at the surface of the cluster. The problem then possesses

the axial symmetry so that the electron ejection position is defined by the angle θ as sketched in panel (a) of the same figure, and φ angle can be set equal to zero. Figure 4(b) presents an ensemble of streaking curves for electrons ejected with a fixed initial velocity $u = 2$ au toward the detector. The results are reported prior to averaging over possible electron energies within the spectral width of the atto-second pulse. The color scale corresponds to the weight of different initial positions. It is given by the $\sin\theta$ dependence. This is a pure statistical factor, which reflects the number of equivalent emitters at the corresponding portion of the surface of the cluster with an area given by $\sigma = 2\pi R_{\rm cl}^2 \sin\theta\, {\rm d}\theta$. Thus, the electron signal from small θ, i.e. from the portion of the cluster surface close to the direction of the detector, is substantially smaller than the signal from the peripheral points at $\theta = \pi/2$.

As it follows from equation (13), for the dipolar plasmon mode the induced field at the cluster surface at $\theta = 0$ is always the opposite of the induced field at $\theta = \pi/2$. Starting from $t_{\rm d} = 250$ au, the induced field of the gold nano-sphere dominates the total IR field. The $\theta = \pi/2$ and $\theta = 0$ streaking curves delimiting the spectra appear then to oscillate in opposite phases, reflecting opposite orientation of the dipolar fields at the corresponding areas of the surface. For smaller $t_{\rm d}$, the relative phase of the $\theta = \pi/2$ and $\theta = 0$ oscillations is influenced by the incident IR field $F_{\rm L}$. The amplitude of the energy oscillations is essentially larger for emission points close to the z-axis ($\theta \to 0$) although the contribution of these electrons to the total yield is small. The incident IR field enhancement is of the order of 5 at this portion of the surface, as can be obtained from equations (11) and (13). The same order of the field enhancement can be also deduced from a comparison of the free-atom results in figure 1 and $\theta \to 0$ streaking curves in figure 4. For the electrons emitted at $\theta = \pi/2$ the induced IR field is twice as small and the total incident field enhancement at the cluster surface is of the order of 1.5, which reduces the amplitude of the energy oscillations in the streaking curve. The difference by a factor of 2 in the amplitude as well as opposite directions of the induced fields at the cluster surface for $\theta = \pi/2$ ($z = 0$, $x^2 + y^2 = R_{\rm cl}^2$) and for $\theta = 0$ ($z = R_{\rm cl}$, $x = y = 0$) is particularly clearly seen for time delay $t_{\rm d} > 420$ au. The incident IR pulse is then terminated, and the IR field acting on the ejected electron is fully determined by the induced dipolar plasmon resonance. Despite the off-resonance conditions (the frequency of the IR pulse is $\omega = 1.6$ eV, while the frequency of the dipolar plasmon is $\Omega = 2.0$ eV), the nano-particle plasmon is excited because of the finite width of the spectrum of the incident IR pulse.

The calculation shows that all the streaking curves almost cross at well-defined delay times. The electron energies at these $t_{\rm d}^{(j)}$ points are very close to the free-atom case shown in figure 1. Therefore, independently of the emission point at the surface, the electron energy change by the induced field due to the nano-sphere plasmon resonance is nearly zero when $t_{\rm d} = t_{\rm d}^{(j)}$. This can be explained with the simplified qualitative treatment. Assuming constant electron velocity u along the trajectory, for the emission at the instant $t_{\rm d}$ the energy change due to the induced field is given by (cf equation (13))

$$\Delta E = -u \int_{t_{\rm d}}^{\infty} \hat{\mathbf{e}}_z \cdot \mathbf{F}_{\rm ind}(x_0,\, y_0,\, z_0 + u(t - t_{\rm d}),\, t)\, {\rm d}t, \tag{14}$$

where (x_0, y_0, z_0) is the emission point at the surface of the cluster. During one period of the IR field, an electron with $u = 2$ au travels approximately 10 nm. This is smaller than the cluster radius and the characteristic scale of the coordinate dependence in $\mathbf{F}_{\rm ind}$ variation. The nodal structure in the $t_{\rm d}$ dependence of the integral in equation (14) is then related with the time variation of the induced dipole and appears to be independent of the emission point.

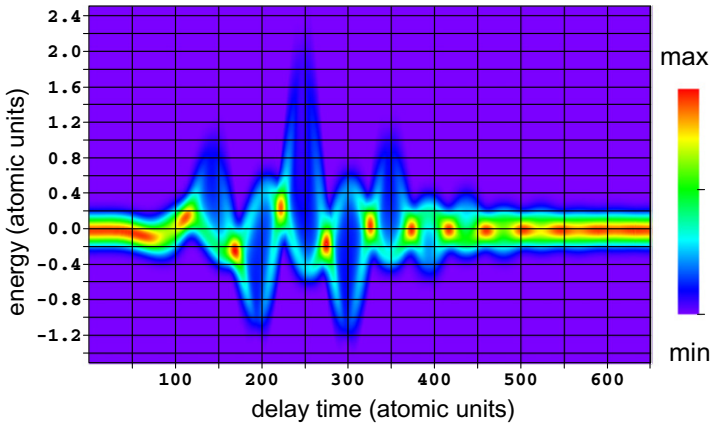

Figure 5. Final streaking spectrogram for the spherical gold cluster with radius $R_{\rm cl} = 50\,\text{nm}$. The energy spectrum of ejected electrons is shown as a function of the delay time $t_{\rm d}$. The energies are given with respect to the central line $E_{\rm f} = 2\,\text{au}$. The color code defines the intensity of the signal as shown in the inset.

We have computed $\int_{t_{\rm d}}^{\infty} P(t)\,{\rm d}t$ and observed that the points $t_{\rm d}^{(j)}$ are very close to the nodes of this quantity. Thus, the correlation has been confirmed with an accuracy that seems to be surprisingly high.

The calculated final streaking spectrogram is presented in figure 5 for the spherical gold cluster with radius $R_{\rm cl} = 50\,\text{nm}$. It is obtained including the emission energy statistics determined by the Gaussian shape of the XUV atto-pulse, and the averaging over possible positions of the emitter at the cluster surface. We account for the position dependence of the electron emission probability in the direction of the detector. It is given by $|\mathfrak{F}(\theta, \varphi)|^2$, where $\mathfrak{F}(\theta, \varphi)$ is the amplitude of the z-component of the XUV field at the surface of the cluster. It is calculated from the classical Maxwell equations using the boundary element method as implemented with the BEMAX code [62, 63]. The dielectric constant of gold for 100 eV photons, $\varepsilon = 0.82 + {\rm i}0.073$, has been taken from synchrotron radiation scattering data [64]. It is worth mentioning that for the spherical clusters with $R_{\rm cl} = 50$ and 20 nm considered in this study, using a homogeneous distribution of the XUV field at the cluster surface $\mathfrak{F}_{\rm as} = \text{const}$ provides very similar streaking spectrograms.

The dependence of streaking on the electron ejection point results in the streaking spectrogram for the spherical gold cluster, which has a much more complex structure than the free-atom and rectangular nano-antenna cases. Because of a larger number of emitters, the electrons ejected from the surface atoms at $\theta \approx \pi/2$ provide a leading contribution to the signal. However, the contribution from the electrons emitted at $\theta \approx 0$, i.e. from the portion of the surface directly facing the detector, is also visible. Basically, all the features discussed with figure 4, including the opposite signs of energy oscillations at small θ and $\theta = \pi/2$, can be seen in the final result. In particular, the $t_{\rm d}^{(j)}$ points of the vanishing induced-field contribution to the final electron energy produce the bright spots in the streaking spectrogram. This provides a good reference for the discussion of the dynamics of the induced field, including the phase shift with respect to the incident IR field. In the present case, plasmonic oscillations decay with a rate $\Gamma/2 = 0.25\,\text{eV}$. Even though less long-lasting than the nano-antenna case, the features of

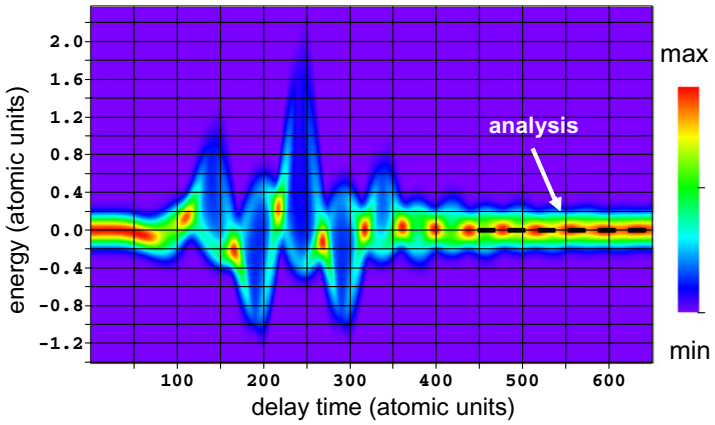

Figure 6. The final streaking spectrogram for the spherical gold cluster with radius $R_{cl} = 20\,\text{nm}$. The energy spectrum of ejected electrons is shown as a function of the delay time t_d. The energies are given with respect to the central line $E_f = 2\,\text{au}$. The color code defines the intensity of the signal as shown in the inset. At large delay times the period and decay rate of the dipolar plasmonic mode of the nano-object can be extracted from the streaking spectrogram analyzing the intensity along the segment shown in black in the figure.

the streaking spectra are well resolved for t_d up to 600 au, i.e. long after the termination of the incident IR pulse.

The conditions for the observation of the induced plasmonic field after the termination of the driving IR pulse are met even better with smaller size spherical nano-clusters owing to the reduced plasmon damping rate. In figure 6, we show the streaking spectrogram for the $R_{cl} = 20\,\text{nm}$ gold nano-sphere. The main features of the calculated results are similar to that discussed above for the $R_{cl} = 50\,\text{nm}$ cluster. In particular, note the following.

1. The energy oscillations are larger than in the free-atom case, indicating plasmonic field enhancement at the cluster surface.
2. The streaking spectra show a complex structure arising from the dependence of the 'probed' induced fields on the electron ejection point at the surface of the cluster.
3. The streaking for the electrons emitted from the portion of the cluster surface at small θ is nearly twice as large as that for $\theta \approx \pi/2$, and the corresponding energy oscillations with delay time are in the opposite phase.
4. Because of the larger number of emitters, the intensity is dominated by the electrons ejected at $\theta \approx \pi/2$.
5. The vanishing contribution from the induced cluster field at well-defined delay times $t_d^{(j)}$ results in periodically spaced bright spots in the spectrogram. The streaking curves for the electrons ejected at different locations at the cluster surface coalesce at $t_d^{(j)}$ with the final electron energy determined by the incident IR field. The locations in time of the bright spots in the streaking spectra allow the observation of the relative phase between the induced dipole and the driving incident IR field.

For $R_{cl} = 20\,\text{nm}$ and $R_{cl} = 50\,\text{nm}$ nano-spheres, the well-resolved structure of the streaking spectra for delay times $t_d > 420\,\text{au}$ (after the termination of the incident IR pulse) allows one

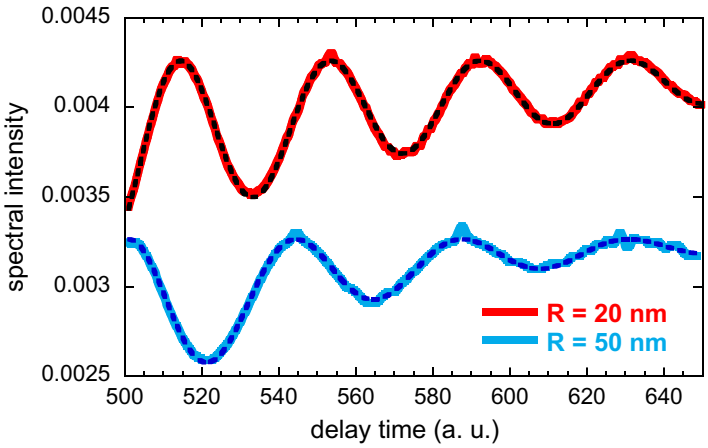

Figure 7. Analysis of the streaking spectrogram for the $R_{\rm cl} = 20\,$nm and $R_{\rm cl} = 50\,$nm spherical gold clusters, allowing us to extract the frequency and the decay rate of the dipolar plasmon mode. Continuous lines show the intensity of the calculated streaking spectrogram along the segment of the central line $E_{\rm f} = 2\,$au, as shown in black in figure 6. Dashed lines: analytical fit to the streaking data. For further details, see the main text.

to extract the plasmon characteristics. An example of possible analyses of the data is shown in figures 6 and 7. The intensity I of the electron energy spectrum is recorded along the central line $E = E_{\rm f}$ as a function of the delay time for large $t_{\rm d} > 500\,$au. In these conditions, I is determined by the central part close to the maximum of the frequency spectrum of the atto-second XUV pulse. Then, the data can be fitted with $I = I_0 - I_1 \exp(-\Gamma_{\rm fit} t)\cos^2(\Omega_{\rm fit} t + \phi)$ dependence. For $R_{\rm cl} = 20\,$nm the fit gives the decay rate $\Gamma_{\rm fit} = 0.27\,$eV and $\Omega_{\rm fit} = 2.19\,$eV. These values are in close agreement with damping $\Gamma = 0.3\,$eV and frequency $\Omega = 2.2\,$eV used to describe the nano-particle response in equation (11). Similarly, for $R_{\rm cl} = 20\,$nm we obtain $\Gamma_{\rm fit} = 0.45\,$eV and $\Omega_{\rm fit} = 1.98\,$eV to be compared with exact $\Gamma = 0.5\,$eV and $\Omega = 2.0\,$eV.

4. Conclusions

In conclusion, in this proof-of-principle work we have presented a theoretical analysis of the atto-second streaking technique when applied to metallic nano-objects. Particular emphasis is given to the characterization of the time dynamics of the dipolar plasmonic near-field. With examples of a gold rectangular nano-antenna and spherical gold clusters we have shown that ASS not only allows direct observation of the time evolution of the induced field, but also allows a rather complete characterization of the plasmonic mode excited by the external IR field. The near-field enhancement, frequency, decay rate and phase of the plasmon oscillations can be measured directly in the time domain. Our study also reveals the role of the spatial inhomogeneity of the induced fields. We show that different orientations of the induced dipolar fields above different patches of the surface of the nano-cluster lead to a rather complex streaking spectrogram which is much different from the well-documented free-atom case. At this point it is worth noting that the spherical cluster example considered here is representative also of possible studies of metallic nano-shells. Based on our results, the ASS has great potential to become an important tool for investigating the plasmonic dynamics of nano-objects.

Acknowledgments

T V Teperik is gratefully acknowledged for providing BEMAX data on XUV scattering from spherical clusters. AKK gratefully acknowledges the hospitality of ISMO.

References

[1] Kelly L, Coronado E, Zhao L L and Schatz G C 2003 *J. Phys. Chem.* B **107** 668
[2] Alvarez-Puebla R, Liz-Marzán L M and García de Abajo F J 2010 *J. Phys. Chem. Lett.* **1** 2428
[3] Link S and El-Sayed M A 2000 *Int. Rev. Phys. Chem.* **19** 409
[4] Hutter E and Fendler J H 2004 *Adv. Mater.* **16** 1685
[5] Gramotnev D K and Bozhevolnyi S I 2010 *Nature Photonics* **4** 83
[6] Schuller J A, Barnard E S, Cai W, Jun Y C, White J S and Brongersma M L 2010 *Nature Mater.* **9** 193
[7] Halas N J, Lal S, Chang W-S, Link S and Nordlander P 2011 *Chem. Rev.* **111** 3913
[8] Akimov A V, Mukherjee A, Yu C L, Chang D E, Zibrov A S, Hemmer P R, Park H and Lukin M D 2007 *Nature* **450** 402
[9] Ozbay E 2006 *Science* **311** 189
[10] Mühlschlegel P, Eisler H-J, Martin O J F, Hecht B and Pohl D W 2005 *Science* **308** 1607
[11] Bharadwaj P, Deutsch B and Novotny L 2009 *Adv. Opt. Photonics* **1** 438
[12] Taminiau T H, Stefani F D, Segerink F B and van Hulst N F 2008 *Nature Photonics* **2** 234
[13] Greffet J J, Laroche M and Marquier F 2010 *Phys. Rev. Lett.* **105** 117701
[14] Mayer K M, Hao F, Lee S, Nordlander P and Hafner J H 2010 *Nanotechnology* **21** 255503
[15] Brongersma M L, Hartman J W and Atwater H A 2000 *Phys. Rev.* B **62** R16356
[16] Citrin D S 2004 *Nano Lett.* **4** 1561
[17] Sainidou R and Garca de Abajo F J 2008 *Opt. Express* **16** 4499
[18] Stockman M I, Faleev S V and Bergman D J 2002 *Phys. Rev. Lett.* **88** 067402
[19] Aeschlimann M, Bauer M, Bayer D, Brixner T, García de Abajo F J, Pfeiffer W, Rohmer M, Spindler C and Steeb F 2007 *Nature* **446** 301
[20] Volpe G, Molina-Terriza G and Quidant R 2010 *Phys. Rev. Lett.* **105** 216802
[21] Greffet J J and Carminati R 1997 *Prog. Surf. Sci.* **56** 133
[22] Ghenuche P, Cherukulappurath S, Taminiau T H, van Hulst N F and Quidant R 2008 *Phys. Rev. Lett.* **101** 116805
[23] Douillard L, Charra F, Korczak Z, Bachelot R, Kostcheev S, Lerondel G, Adam P M and Royer P 2008 *Nano Lett.* **8** 935
[24] Schnell M, Garcia-Etxarri A, Huber A J, Crozier K, Aizpurua J and Hillenbrand R 2009 *Nature Photonics* **3** 287
[25] García de Abajo F J 2010 *Rev. Mod. Phys.* **82** 209
[26] Klein-Wiele J-H, Simon P and Rubahn H-G 1998 *Phys. Rev. Lett.* **80** 45
[27] Lamprecht B, Krenn J R, Leitner A and Aussenegg F R 1999 *Phys. Rev. Lett.* **83** 4421
[28] Scharte M, Porath R, Ohms T, Aeschlimann M, Krenn J R, Ditlbacher H, Aussenegg F R and Liebsch A 2001 *Appl. Phys. B: Lasers Opt.* **73** 305
[29] Kubo A, Onda K, Petek H, Sun Z, Jung Y S and Kim H K 2005 *Nano Lett.* **5** 1123
[30] Kubo A, Pontius N and Petek H 2007 *Nano Lett.* **7** 470
[31] Link S and El-Sayed M 2003 *Annu. Rev. Phys. Chem.* **54** 331
[32] Hentschel M, Kienberger R, Spielmann Ch, Reider G A, Milosevic N, Brabec T, Corkum P, Heinzmann U, Drescher M and Krausz F 2001 *Nature* **414** 509
[33] Drescher M, Hentschel M, Kienberger R, Uiberacker M, Yakovlev V S, Scrinizi A, Westerwalbesloh T, Kleineberg U, Heinzmann U and Krausz F 2002 *Nature* **419** 803
[34] Itatani J, Quere F, Yudin G L, Ivanov M Y, Krausz F and Corkum P B 2002 *Phys. Rev. Lett.* **88** 173903

[35] Kitzler M, Milocevic N, Scrinzi A, Krauzs F and Brabec T 2002 *Phys. Rev. Lett.* **88** 173904
[36] Kienberger R *et al* 2002 *Science* **297** 1144
[37] Kienberger R and Krausz F 2004 *Phys. Scr.* **T110** 32
[38] Kienberger R *et al* 2004 *Nature* **427** 817
[39] Kazansky A K and Kabachnik N M 2007 *J. Phys. B: At. Mol. Opt. Phys.* **40** 2163
[40] Krausz F and Ivanov M 2009 *Rev. Mod. Phys.* **81** 163
[41] Uiberacker M *et al* 2007 *Nature* **446** 627
[42] Uphues Th, Schultze M, Kling M F, Uiberacker M, Hendel S, Heinzmann U, Kabachnik N M and Drescher M 2008 *New J. Phys.* **10** 025009
[43] Kazansky A K and Kabachnik N M 2007 *J. Phys. B: At. Mol. Opt. Phys.* **40** F299
Kazansky A K and Kabachnik N M 2008 *J. Phys. B: At. Mol. Opt. Phys.* **41** 135601
[44] Cavalieri A L *et al* 2007 *Nature* **449** 1029
[45] Sansone G *et al* 2010 *Nature* **465** 763–6
[46] Kazansky A K, Sazhina I P and Kabachnik N M 2009 *Tech. Phys.* **54** 333
[47] Powell C J and Jablonski A 1999 *J. Phys. Chem. Data* **28** 19
[48] Kazansky A K and Echenique P M 2009 *Phys. Rev. Lett.* **102** 177401
[49] Borisov A G and Shabanov S V 2005 *J. Comput. Phys.* **209** 643
[50] Kreiter M, Mittler S, Knoll W and Sambles J R 2002 *Phys. Rev.* B **65** 125415
[51] Stockman M I, Kling M F, Kleineberg U and Krausz F 2007 *Nature Photonics* **1** 539
[52] Stockman M I 2008 *New J. Phys.* **10** 025031
[53] Sönnichsen C, Franzl T, Wilk T, von Plessen G and Feldmann J 2002 *New J. Phys.* **4** 93.1
[54] Myroshnychenko V, Rodríguez-Fernández J, Pastoriza-Santos I, Funston A M, Novo C, Mulvaney P, Liz-Marzán L M and García de Abajo F J 2008 *Chem. Soc. Rev.* **37** 1792
[55] Mie G 1908 *Ann. Phys. Lpz* **25** 377
[56] Link S and El-Sayed M A 2000 *Int. Rev. Phys. Chem.* **19** 409
[57] Prodan E and Nordlander P 2003 *Nano Lett.* **3** 543
[58] Prodan E, Radloff C, Halas N J and Nordlander P 2003 *Science* **302** 419
[59] Prashant J K, Lee K S, El-Sayed I H and El-Sayed M A 2006 *J. Phys. Chem.* B **110** 7238
[60] Lal S, Link S and Halas N J 2007 *Nature Photonics* **1** 641
[61] Averitt R D, Westcott S L and Halas N J 1999 *J. Opt. Soc. Am.* B **16** 1824
[62] García de Abajo F J and Howie A 1998 *Phys. Rev. Lett.* **80** 5180
[63] García de Abajo F J and Howie A 2002 *Phys. Rev.* B **65** 115418
[64] Wolf R, Birken H-G, Blessing C and Kunz C 1994 *Appl. Opt.* **33** 2683